Low-complexity R-peak detection for ambulatory fetal monitoring

Michael J. Rooijakkers, Chiara Rabotti, S. Guid Oei, and Massimo Mischi

M.J. Rooijakkers, C. Rabotti and M. Mischi are with the Faculty of Electrical Engineering, University of Technology Eindhoven, 5612 AZ, Eindhoven, The Netherlands

S.G. Oei is with the Department of Obstetrics and Gynecology, Máxima Medical Center, 5500 MB Veldhoven, The Netherlands

E-mail: `m.j.rooijakkers@tue.nl`

Abstract.

Non-invasive fetal health monitoring during pregnancy is becoming increasingly important because of the increasing number of high-risk pregnancies. Despite recent advances in signal processing technology, which have enabled fetal monitoring during pregnancy using abdominal ECG recordings, ubiquitous fetal health monitoring is still unfeasible due to the computational complexity of noise-robust solutions. In this paper, an ECG R-peak detection algorithm for ambulatory R-peak detection is proposed, as part of a fetal ECG detection algorithm. The proposed algorithm is optimized to reduce computational complexity, without reducing the R-peak detection rate compared to existing R-peak detection schemes. Validation of the algorithm is performed on three manually annotated datasets. With a detection error rate of 0.23%, 1.32%, and 9.42% on the MIT/BIH Arrhythmia and in-house maternal and fetal databases, respectively, the detection rate of the proposed algorithm is comparable to the best state-of-the-art algorithms, at a reduced computational complexity.

Keywords: electrocardiography, R-peak detection, abdominal measurements, fetal ECG, wavelet transform, adaptive signal processing.

1. INTRODUCTION

Fetal heart rate (fHR) monitoring and derivation of the fetal electrocardiogram (fECG) are important means to assess fetal distress during pregnancy and delivery (Amer-Wahlin et al. 2001, Vullings et al. 2009). Currently used methods are however not suited for long term observation throughout pregnancy. The most commonly used methods for fHR monitoring either use Doppler ultrasound or a fetal scalp electrode. While allowing for non-invasive measurements, Doppler ultrasound measurements introduce energy into the body and need continuous attention of a trained physician, making them unsuitable for long term observation (Peters et al. 2001, Kieler et al. 2001). Furthermore, these measurements do not provide conclusive information for accurate assessment of fetal health and, therefore, additional information is needed for clinical decisionmaking (Amer-Wahlin et al. 2001). FHR monitoring using an invasive scalp electrode (Hon et al. 1972), while giving very accurate electrocardiogram (ECG) readings and an instantaneous fHR measurement (Peters et al. 2001), needs rupturing of the membranes and can therefore only be applied during delivery. Because of the invasiveness of the procedure, relying on a needle-like electrode which is screwed into the scalp to obtain the fECG signal, there is a risk of infection and tissue damage (Taylor et al. 2005). Widespread use of fetal scalp electrodes may therefore not be acceptable to obstetricians or to mothers.

Electrophysiological measurements on the maternal abdomen also contain the fECG and enable extraction of both the fHR and cleaned fECG. However, the signal has a reduced SNR compared to the use of a fetal scalp electrode, with the maternal electrocardiogram (mECG) as the predominant interference. Over the last few decades various methods for fECG extraction have been published which can be subdivided in spatial filtering (Bergveld & Meijer 1981), adaptive filtering (Widrow et al. 1975, Strobach et al. 1994), template subtraction (Ungureanu et al. 2007, Vullings et al. 2009), and independent component analysis (ICA) (Taylor et al. 2003). Because of the high quality results compared to other methods, e.g. spatial and adaptive filtering, template subtraction, and ICA, we used the weighted averaging of mECG segments (WAMES) method proposed in (Vullings et al. 2009) as a baseline reference. The WAMES method removes the mECG to increase the signal-to-noise ratio (SNR) implementing the following steps: 1) preprocessing, 2) maternal R-peak detection, 3) mECG estimation, and 4) mECG subtraction. The resulting signal can be used for fetal R-peak detection with results comparable to those obtained using a scalp electrode (Vullings et al. 2009). Continuous monitoring of the fetus in an ambulatory setting using this method is however still unfeasible, due to its computational complexity.

In an effort to reduce the complexity and increase the HR detection quality of (Vullings et al. 2009), we propose an algorithm to replace the R-peak detection algorithm used in (Vullings et al. 2009), which is based on (Gritzali 1988). The preprocessing stage of (Gritzali 1988) contains a length transform, composed of consecutive differentiation, absolute value, and integrator stages, to emphasize the features of the QRS complex.

Because of the high-pass filtering effect of the differentiation, the method described in (Gritzali 1988) is very sensitive to measurement noise and requires pre-filtering, especially on measurements obtained in an ambulatory setting. Therefore, a single FIR filter with a length of 0.5 s is used in (Vullings et al. 2009), combining a high-pass (HP) and low-pass (LP) filter at 2.5 Hz and 25 Hz, respectively. The decision stage is based on thresholding, where the height of the threshold is dependent on the local absolute signal amplitude of the preprocessed waveform.

To allow for comparison between the proposed algorithm and algorithms from literature, a dataset of thoracic measurements and two abdominal datasets, containing maternal and fetal ECG measurements respectively, are used. The proposed R-peak detection algorithm, which is based on the discrete-time continuous wavelet transform (DT-CWT), reduces the overall computational complexity, while increasing the R-peak detection quality of the maternal ECG.

After a short introduction of the DT-CWT, the proposed R-peak detection algorithm is described in Section 2. Section 3 introduces and describes implementation details of several algorithms from the literature, which are used for comparison. Section 4 discusses the recordings used for validation as well as details on the methodology of this comparison. The comparison results are shown in Section 5, followed by a discussion and conclusion in Section 6.

2. R-PEAK DETECTION ALGORITHM

Algorithm design for detection of the QRS interval in an ECG signal has been a topic of research for the past four decades, and a large number of algorithms exist of which an overview is given in (Kohler et al. 2002). The most promising group of algorithms is based on the wavelet transform, an approach which has been widely investigated, e.g. in recent studies by (Li et al. 1995, Martinez et al. 2000, Romero Legarreta et al. 2005, Romero et al. 2009). These studies show that wavelet-based algorithms provide high detection quality at low computational complexity. The DT-CWT has proven to be of particular interest to measurements obtained in an ambulatory setting, giving an overall superior performance compared to discrete wavelet transform based methods (Romero et al. 2009, Yoon et al. 2010).

Based on the DT-CWT as described in Section 2.1 and a selection of wavelets as described in Section 2.1.1, a new R-peak detection algorithm was designed. The algorithm can be divided in a number of successive steps, grouped in preprocessing and R-peak detection stages, as shown in the block-diagram in Fig. 1.

2.1. Discrete-Time Continuous Wavelet Transform

A wavelet function $\varphi[n]$ can be any localized waveform which has finite energy and a zero mean (Addison 2002). We can then define the DT-CWT of a signal $x[n]$ with

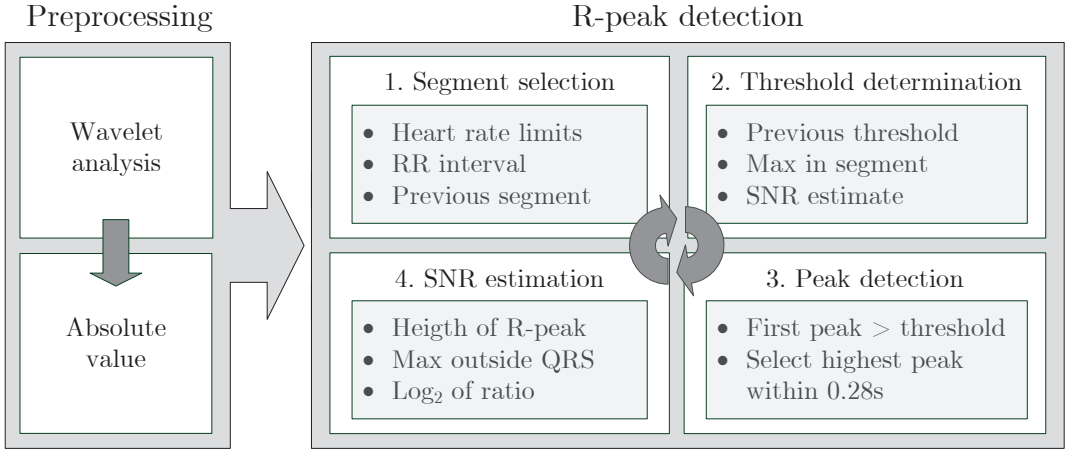

Figure 1. Block-diagram of the proposed R-peak detection algorithm.

respect to a wavelet function $\varphi[n]$ as:

$$CWT_s[\tau] = \frac{1}{\sqrt{s}} \sum_{n=-\infty}^{\infty} x[n] \cdot \varphi\left[\frac{n-\tau}{s}\right], \tag{1}$$

where the 'translation' parameter τ gives the location in time and the 'dilation' parameter s is a scaling factor. The peak frequency of the wavelet's band-pass filtering effect, which is characterized by the energy spectrum of the wavelet function $\varphi[n]$, can be altered by changing s. The wavelet's peak frequency f_p depends on the wavelet scale s and the signal sampling frequency f_s as follows:

$$f_p = \frac{s_{f_c} \cdot f_s}{s}, \tag{2}$$

where s_{f_c} is the relative characteristic (peak) frequency of a specific wavelet.

2.1.1. Wavelet options Some wavelets which are commonly used for R-peak detection in ECG measurements are the Haar, Morlet, Gaussian wave and Mexican hat wavelets, the latter two being the first and second derivative of the Gauss function, respectively (Addison 2002). These wavelets are described by the following functions:

Haar
$$\varphi[n] = \begin{cases} 1 & -1/2 \le t \le 0 \\ -1 & 0 \le t \le 1/2 \\ 0 & \text{otherwise} \end{cases} \tag{3}$$

Gaussian wave
$$\varphi[n] = -n \cdot e^{-\frac{n^2}{2}}, \tag{4}$$

Mexican Hat
$$\varphi[n] = (1 - n^2) \cdot e^{-\frac{n^2}{2}}, \tag{5}$$

Morlet
$$\varphi[n] = \cos 5n \cdot e^{-\frac{n^2}{2}}, \tag{6}$$

where n is the sample index.

Table 1. R-peak detection quality results on the MIT/BIH Arrhythmia database for four different wavelets after optimization. For each wavelet Sensitivity (S_e), Positive predictivity ($+P$), D_e, peak frequency (f_p), and Δ_s^r of the optimal solution are given.

	Se (%)	$+P$ (%)	D_e (%)	f_p (Hz)	Δ_s^r
Haar	99.73	99.76	0.50	21	0.7
Gaussian wave	99.75	99.78	0.47	18	0.7
Mexican hat	**99.87**	**99.90**	**0.23**	**18**	**1**
Morlet	99.60	99.83	0.57	18	3

Fig. 2 shows the function waveforms in the time domain as well as their respective magnitude spectra. The maximum in each of the magnitude spectra, is defined by the relative characteristic frequency s_{f_c}, which is $\frac{3}{4}$, $\frac{1}{2\pi}$,$\frac{\sqrt{2}}{2\pi}$, and $\frac{4}{5}$ for the Haar, Gaussian wave, Mexican hat, and Morlet wavelets, respectively (Addison 2002).

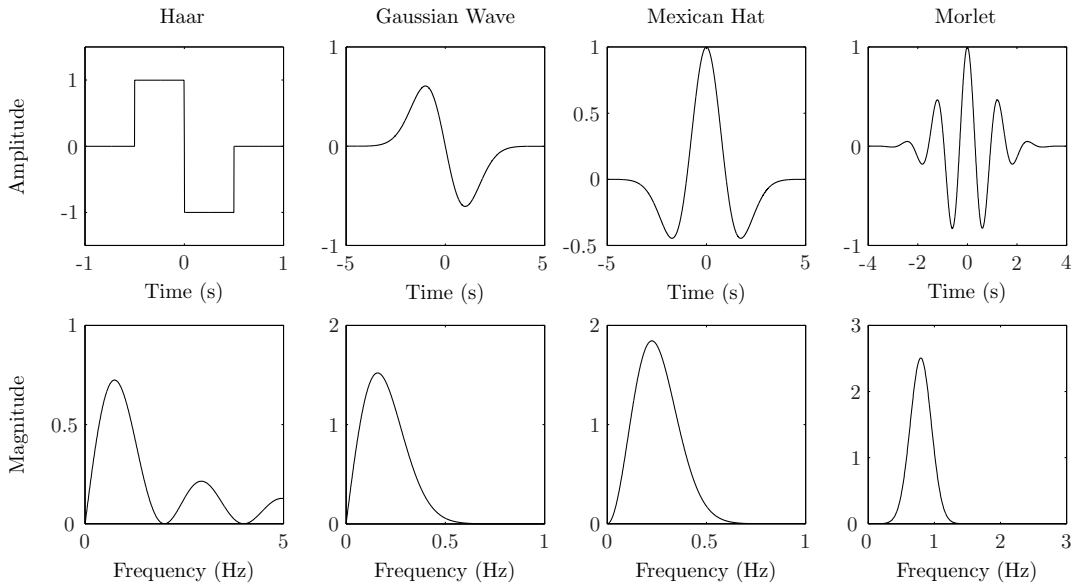

Figure 2. The top row shows from left to right plots of the Haar, Gaussian wave, Mexican hat, and Morlet wavelets for normalized time. The bottom row gives their respective magnitude spectra.

2.1.2. Wavelet choice For the final wavelet analysis implementation, a single wavelet was chosen based on the quality of R-peak detection, as defined in Section 4.2. To this end, the R-peak detection algorithm, as proposed in Section 2.3, was used on the MIT/BIH Arrhythmia database (MITDB) (Moody 1997) for each of the wavelets described above. Table 1 shows the detection error rate (D_e) and the relative support width (Δ_s^r), which is indicative of the computational complexity, for each of the wavelets after optimization.

Using the Haar or Gaussian wave wavelet, gives two peaks of similar height for each R-peak in the preprocessed signal. The Morlet wavelet introduces even more

peaks, making selecting the correct peak more difficult. Therefore, using the Mexican hat wavelet results in a markedly lower D_e compared to the other wavelets, although all wavelets have a similar magnitude spectrum. Because the Mexican hat wavelet achieves the lowest D_e, with Δ_s^r only slightly higher than that of the Haar and Gaussian wave wavelets, this wavelet is selected for use in the R-peak detection algorithm.

2.2. Preprocessing

The preprocessing stage consists of a DT-CWT of the ECG signal with the Mexican hat wavelet, which is used in the range $\Delta n = [-4,\ 4]$. This results in a minimal computational complexity while retaining the required accuracy at the edges. To further reduce the computational complexity of the algorithm, only a single scale s is used in the wavelet analysis. The peak frequency f_p of the wavelet is chosen at 18 Hz, centered in the $10-25$ Hz frequency band, which contains most of the QRS energy of the mECG (Kohler et al. 2002). This reduces the DT-CWT to a convolution with a single wavelet, which has a support width $\Delta_s = \Delta n \cdot s_{f_c}/f_p = 97$ ms. In case of a sampling frequency $f_s = 360$ Hz, as used in the MIT/BIH arrhythmia database introduced in Section 4, this results in the wavelet coefficients as shown in Fig. 3.

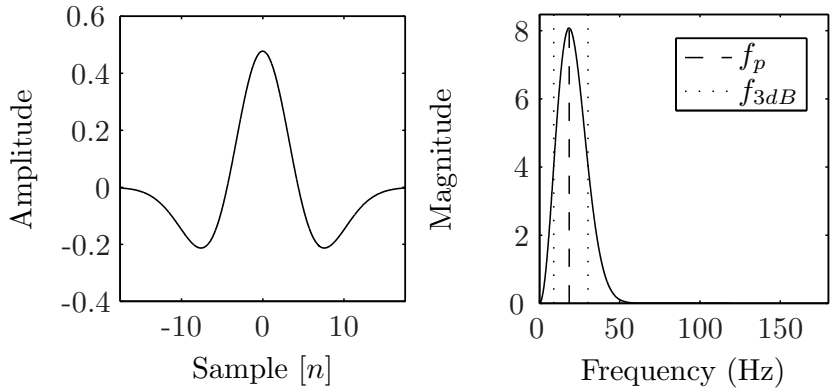

Figure 3. Plot of Mexican hat wavelet (left) and its magnitude spectrum (right), where $f_s = 360$ Hz and $f_p = 18$ Hz.

Subsequently the absolute value of the wavelet analysis output is taken, resulting in the output signal S. Taking the absolute value allows for the use of a single threshold in the following R-peak detection stage, independent of the orientation of the cardiac vector with respect to the electrode position. This will prove to be especially useful for the fECG, since the orientation of the fetal heart is a-priori unknown, and can change in the course of a measurement.

2.3. R-Peak detection

The R-peak detection part of the algorithm consists of four consecutive stages, which are executed in an iterative fashion, as shown in the right part of Fig. 1. These stages

are, in order, 1) segment selection, 2) threshold determination, 3) peak detection and 4) SNR estimation.

2.3.1. Segment selection In each iteration of the algorithm, a signal segment (δS) is chosen such that the segment is expected to contain exactly one R-peak. Different from (Madeiro et al. 2007), where segment selection is used to reduce the computational complexity, this is done to increase the quality of the subsequent threshold determination in preparation of the following R-peak detection. The increase in detection quality is achieved because a better threshold determination is possible, especially for ECG signals with fast changes in QRS amplitude, as the threshold is updated based on a single QRS complex only. To this end, the limits for the next segment are selected based on previously found R-peak positions and the assumption that the HR is in the range of 32 - 210 beats per minute (BPM) (Robergs & Landwehr 2002). This gives the following set of equations defining the start δS_s and the end δS_e of the current signal segment $\delta S\,[n]$, respectively:

$$\delta S_s\,[n] = \widehat{p}\,[n-1] + RR_{min}, \tag{7}$$

$$\delta S_e\,[n] = \delta S_s + \min\left\{\beta \cdot \left(\widehat{p}\,[n-1] - \widehat{p}\,[n-2]\right), RR_{max}\right\}, \tag{8}$$

where, RR_{min} and RR_{max} are the minimal and maximal RR-intervals defined by the allowed HR range, $\widehat{p}\,[n]$ gives the time-stamp of the n^{th} detected R-peak, and β defines the relative length of δS. Compared to the last RR-interval, β can be anywhere in the range $[1.3, 1.7]$. However, since a longer segment reduces the number of false positive detections, $\beta = 1.7$ is selected, as the application of the algorithm will be in an ambulatory setting resulting in noisy recordings. The total length of δS is limited by RR_{max} to ensure no run away situations will occur.

2.3.2. Threshold determination For each signal segment δS, a threshold value T is calculated based on the previous threshold value T_{prev} and a new threshold estimate $\widehat{T}$, using the following first-order auto regressive (AR(1)) process:

$$T = \alpha \cdot \widehat{T} + (1-\alpha) \cdot T_{prev}, \tag{9}$$

where α describes the dynamic behavior of the threshold. The optimal value of $\alpha = 1/3$, which was found experimentally, allows the threshold to follow amplitude changes in the QRS-complexes due to breathing. In (9), $\widehat{T} = N_l \cdot S_{max}$, where S_{max} is the maximum value in the current preprocessed signal segment and N_l is the estimated local noise level as defined in Section 2.3.4. To reduce the number of falsely detected peaks in signal segments without an R-peak present, a lower bound for threshold T is set at four times the mean of the preprocessed signal S.

2.3.3. Peak detection Within the selected signal segment δS, a peak position candidate $\widehat{p}$ at time t is selected as the first preprocessed sample crossing the threshold T. The search segment is now reduced to an interval starting at $\widehat{p}$ with a length of 0.28 s, defined by $\mathrm{HR}_{\max}$, as any peak found outside this interval could be a new R-peak. Within this interval, a new sample $\widehat{p}+i$ is selected as the new $\widehat{p}$ if the peak-amplitude $S\left[\widehat{p}+i\right]$ is higher than that of the last R-peak candidate, i.e.

$$S\left[\widehat{p}+i\right] > S\left[\widehat{p}\right]. \tag{10}$$

It is possible that no R-peak position $\widehat{p}$ is selected in the current segment. In this case, up to two more iterations at the current segment location starting at δS_s are performed. With each iteration the end of the search segment δS_e is extended and a new threshold value T is determined by:

$$\delta S_e = \begin{cases} \frac{\delta S_s + \delta S_e + RR_{max}}{2} & ;\ 2^{nd}\ \text{iteration} \\ \delta S_s + RR_{max} & ;\ 3^{rd}\ \text{iteration} \end{cases}, \tag{11}$$

and

$$T = \alpha \cdot \widehat{T} + (1-\alpha) \cdot \frac{T_{prev}}{2}, \tag{12}$$

respectively, where $\alpha = 1/3$ as defined in Section 2.3.2. If after three iterations no peak is found, a new search is started in a segment δS, which has moved forward 1 s. The example in Fig. 4 first shows an instance, where an R-peak is detected in the third iteration (17 s), and consecutively a case where after three iterations at the same location no peak is found and the search segment is moved forward (19 s).

2.3.4. SNR estimation Once an R-peak has been detected, an estimate of the SNR ($\widehat{\mathrm{SNR}}$) after preprocessing, around the last R-peak position, is calculated. Classically the signal-to-noise ratio is determined by:

$$\mathrm{SNR} = 10 \cdot \log_{10}\left(\frac{P_s}{P_n}\right), \tag{13}$$

where P_s is the signal-power, and P_n is the noise-power. A problem arises when applying such a definition to an ECG signal, as the signal power will be proportional to the square of the heart rate. Such a measure has no relation with R-peak detection. Therefore, P_s and P_n are defined as the maximal power within fixed windows around a detected R-peak and in the segments between consecutive R-peaks, respectively. The resulting expression is given as:

$$\mathrm{SNR} = 10 \cdot \log_{10}\left(\frac{S\left[\widehat{p}\right]^2}{N_{max}^2}\right) = 20 \cdot \log_{10}\left(\frac{S\left[\widehat{p}\right]}{N_{max}}\right), \tag{14}$$

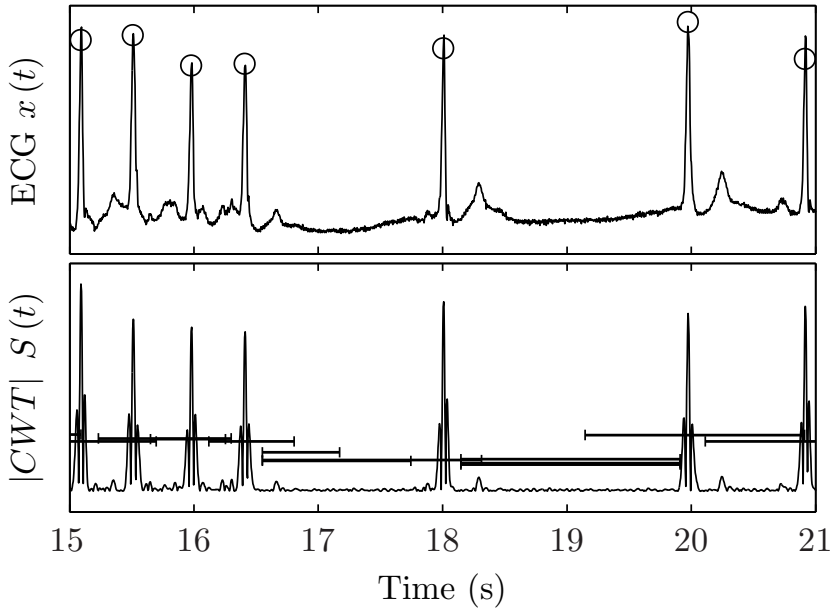

Figure 4. Example of an ECG signal segment (top), where $\odot$ indicates the R-peaks. The horizontal bars in the preprocessed ECG S (bottom) indicate the length of and threshold level for each of the used segments.

where N_{max} is the maximum in S in the two intervals $[\delta S_s, \widehat{p} - 75 \text{ ms}]$ and $[\widehat{p} + 75 \text{ ms}, \widehat{p} + 250 \text{ ms}]$. This is the maximal-length segment without QRS-complex (Pan & Tompkins 1985), taking HR_{max} into account, and assuming correct detection of $\widehat{p}$. In order to reduce this function's computational complexity in integer-based implementations, the decadic logarithm is replaced by a binary logarithm and rewritten giving:

$$\widehat{\text{SNR}} = \log_2\left(S\left[\widehat{p}\right]\right) - \log_2\left(N_{max}\right), \tag{15}$$

which, except for a scaling factor, corresponds to (14), and the obtained SNR estimate $\widehat{\text{SNR}}$ corresponds with a signal quality. For ease of use a noise level N_l indicative of the local SNR is deduced. The noise level N_l is a scaling factor in the range of $[0, 1]$ and defined by:

$$N_l = \frac{\left(6 - \widehat{\text{SNR}}\right)}{8}, \tag{16}$$

where a low value of N_l indicates minimal noise level, while $N_l \geq 6/8$ indicates an $\widehat{\text{SNR}}$ below 0 dB.

3. IMPLEMENTATIONS FROM THE LITERATURE

Apart from the proposed R-peak detection algorithm, three more algorithms from the literature have been implemented in Matlab for comparison on the datasets described

in Section 4.1. Each of the algorithms proposed by (Vullings et al. 2009, Pan & Tompkins 1985, Li et al. 1995), as well as their implementations are shortly discussed in Sections 3.1-3.3. These algorithms were chosen, because (Vullings et al. 2009) is the reference algorithm in the WAMES algorithm, and (Pan & Tompkins 1985, Li et al. 1995) are much cited algorithms optimized for low-power online use, and high detection rate respectively.

3.1. Vullings

The R-peak detection algorithm introduced by Vullings is based on a method using the length transformation as proposed by (Gritzali et al. 1989). In the preprocessing stage, (Vullings et al. 2009) uses a bandpass filter with low and high cut-off frequencies of 2.5 Hz and 25 Hz, respectively, to reduce the influence of noise and artifacts. This filter is implemented by means of a FIR filter with a support width of 0.5 s. Consecutively, the filtered ECG waveform is processed using a length transformation, based on the one proposed in (Gritzali et al. 1989), which in the algorithm by Vullings is defined as:

$$S[n] = \sum_{i=1}^{n+q-1} \sqrt{(x[i+1] - x[i])^2}, \tag{17}$$

where $q = 0.065 \cdot f_s$ defines the used window length, which is approximately equal to the duration of the QRS. Detection of the QRS complexes is based on thresholding. Contrary to (Gritzali et al. 1989), where one out of a set of three fixed thresholds is used based on the absolute amplitude of the signal, an adaptive threshold is updated continuously by means of a Kalman filter. This Kalman filter is defined as:

$$T = T_{prev} + K \cdot \left(0.3 \cdot \max\left\{|\vec{S_\tau}|\right\} - T_{prev}\right), \tag{18}$$

where $|\vec{S_\tau}| = |S[n-\tau]|, ..., |S[n]|$, with τ a time interval corresponding to the most recent RR-interval. The Kalman gain K is defined as:

$$K = \frac{\rho^2}{\rho^2 + \sigma_S^2}, \tag{19}$$

with

$$\rho^2 = \frac{\rho_{prev}^2 \sigma_S^2}{\rho_{prev}^2 + \sigma_S^2} \tag{20}$$

the variance of the estimate of the current threshold T and σ_S^2 the variance of S in the interval $[n-\tau, n]$. The initial value of T is set equal to the variance of $|S|$ in the first 2 s of the filtered signal. R-peak locations are selected by finding the top in each signal segment crossing the local threshold taking a blanking period of 0.25 s after each detected peak into account.

3.2. Pan-Tompkins

In the preprocessing stage of the algorithm proposed by (Pan & Tompkins 1985), the signal passes through a digital bandpass filter composed of cascaded high-pass and low-pass IIR filters, with cut-off frequencies of 5 Hz and 12 Hz, respectively, to attenuate the noise present in the ECG signal. As the algorithm was developed for real time operation on a simple microprocessor, it uses integer arithmetic to reduce the computational complexity. Designing the chosen class of filters with integer coefficients limits the design flexibility greatly. The coefficients as determined by (Pan & Tompkins 1985) for the low-pass and high-pass filters given by

$$x_l[n] = \frac{1}{36}\left(2x_l[n-1] - x_l[n-2] + x[n] - 2x[n-6] + x[n-12]\right), \tag{21}$$

and

$$S_f[n] = \frac{1}{32}\left(-S_f[n-1] - x_l[n] + 32x_l[n-16] + x_l[n-32]\right), \tag{22}$$

respectively, are specifically designed for $f_s = 200$ Hz. Since the filters would need to be redesigned for all $f_s \neq 200$ Hz, all input signals are resampled to 200 Hz before preprocessing. Further steps in the preprocessing stage include differentiation, squaring, and a moving window integration, using a square window of 150 ms, to emphasize the QRS complex.

The R-peak detection stage uses two sets of thresholds to detect QRS complexes, for an improved reliability of detection compared to using one waveform alone. The sets of two thresholds are used for the filtered ECG, and the signal produced by moving window integration, respectively. R-peak detection is performed in segments of 2 s, which start 0.2 s after the last detected R-peak, by finding all indices where both the filtered ECG and the signal after integration cross their respective thresholds. A final choice of R-peak is determined by taking the blanking and searchback requirements posed in (Pan & Tompkins 1985) into consideration. After detection of every peak, both sets of thresholds are updated using all local maxima found after the previous R-peak. In case of an irregular heart rate, both sets of thresholds are reduced by half to increase the detection sensitivity and avoid missing valid R-peaks.

3.3. Li

The algorithm by (Li et al. 1995) is, contrary to the two previously described methods, based on the dyadic grid discrete wavelet transform (DWT) using the quadratic spline wavelet as a wavelet function. Implementation is done recursively without decimation (algorithme à trous) (Addison 2002, Martinez et al. 2004), using a highpass and lowpass filter, defined by:

$$h\left[n\right] = \sum_{i=-\infty}^{\infty} a\left[i\right] \mathrm{sinc}\left[n-i\right], \quad \text{where } a[i] = \begin{cases} 2\ ; & i \cdot 2^{k-1} = 0 \\ -2\ ; & i \cdot 2^{k-1} = 1 \\ 0\ ; & else \end{cases} \tag{23}$$

and

$$l\left[n\right] = \sum_{i=-\infty}^{\infty} a\left[i\right] \mathrm{sinc}\left[n-i\right], \quad \text{where } a[i] = \begin{cases} 1\ ; & i \cdot 2^{k-1} = \{0,3\} \\ 3\ ; & i \cdot 2^{k-1} = \{1,2\} \\ 0\ ; & else \end{cases}, \tag{24}$$

respectively, where k gives the wavelet scale. The wavelet transform output of scales 1 through 4, which corresponds to a total frequency range of 4-125 Hz at $f_s = 250$ Hz as proposed in (Li et al. 1995), is used in the following R-peak detection stage. As the frequency content of the various wavelet scales is determined by f_s and the frequency characteristics of the used wavelet, either the input signal $x\left[n\right]$ or the used wavelets have to be resampled for correct operation on input signals for which $f_s \neq 250$ Hz. Resampling the wavelets, as proposed by (Martinez et al. 2004), yields wavelets with a very long support width, strongly increasing the computational complexity of the algorithm. Therefore, all input signals are resampled to 250 Hz before preprocessing using the DWT.

In the R-peak detection stage, two thresholds for each of the used wavelet scales are used for determination of the modulus maximum lines (MMLs) of the R waves. This is done by selecting all threshold crossings at scale 4 and recursively finding neighboring threshold crossings at lower scales, eliminating MMLs which do not cross the thresholds at all four scales. After calculation of the singular degree α for each MML, MMLs with $\alpha < 0$ are eliminated. Next, isolation MMLs, which are MMLs for which no neighboring MML of the opposite sign is present, and redundant MMLs, where several MMLs are present in the neighborhood of a MML with the opposite sign, are eliminated. Finally 'blanking' and 'searchback' are employed as postprocessing tactics to find the final R-peak locations.

3.4. Algorithm adjustments for fetal R-peak detection

Because the physiology of the fetal heart differs from that of a mature heart, all the algorithms need adjustments for optimal fetal R-peak detection. Two mayor differences between the maternal and fetal ECG are the expected HR and the spectral content of the QRS complex. Recently, fetal HRs of up to 270 BPM have been recorded by (Haritopoulos et al. 2010) and an algorithm allowing for a fHR up to 300 BPM has been described by (Dawes et al. 1990). Current fetal monitoring systems as well as most fetal R-peak detection algorithm, however, assume the fHR in the range of $60 - 240$ BPM (Graatsma et al. 2009, Sahin et al. 2010). For a fetus with a gestational age between 32 to 41 most of the QRS spectral energy is contained in the $20 - 60$ Hz range (Abboud & Sadeh 1989).

The presented algorithm is adjusted by changing the segment selection step accordingly, allowing for fHR detection in the range of $50 - 255$ BPM, and setting the peak frequency in the preprocessing step to $f_p = 44$ Hz. The algorithm by Vullings is adjusted by increasing the low and high cut-off frequencies of the preprocessing stage

to 20 Hz and 60 Hz respectively, while reducing the length transformation to 40 ms. Tuning the algorithms by Pan-Tompkins and Li for detection of fetal QRS complexes is less straight forward due to the discrete nature of the used filtering techniques. Because both the minimal HR, as well as the frequency range of the QRS complex have approximately doubled, in both of these cases the input data can be resampled to compensate for these changes. The optimal sampling frequencies for detection of fetal R-peak were experimentally found to be 400 Hz and 550 Hz for Pan-Tompkins and Li, respectively.

4. VALIDATION

The comparison of algorithm performance was carried out using two important quality measures in ambulatory monitoring: R-peak detection performance and computational complexity.

4.1. Data acquisition and preprocessing

Validation of the algorithm and comparison with other state-of-the-art algorithms from literature was done by comparing the algorithm results with manually annotated R-peak locations on three sets of recordings. These recordings allow for a performance evaluation of maternal R-peak detection on both thoracic and abdominal recordings, as well as fetal R-peak detection rate on an abdominal dataset.

The first of the three datasets consists of the whole MITDB, containing 48 thoracic measurements of 30 min each, sampled at 360 Hz. All recordings in the MITDB contain two ECG leads, of which only the first (MLII) was used for R-peak detection and comparison with state-of-the-art algorithms as described in literature. The whole MITDB was used for validation, with the exception of some segments in record 207, which are annotated to contain ventricular flutter episodes (Martinez et al. 2004, Madeiro et al. 2007).

The second dataset consists of an in-house database (IHDB) with a total length of 9.5 hours, comprising 20 abdominal measurements from eight women during labor at full term ($40d3 \pm 13$). These data were collected at the Máxima Medical Centre in Veldhoven (The Netherlands) as described in (Rabotti et al. 2009). The study was approved by the Ethical Committee of the hospital and all women signed an informed consent. Each measurement in the IHDB was recorded using the electrode configuration shown in Fig. 5, with eight channels, each sampled at 1000 Hz. A set of six bipolar leads, constructed from leads 4 through 7 on the lower abdomen was selected, as this position offers the best fetal ECG measurements and allows for measurement of uterine activity.

The third dataset was created from a subset of the IHDB recordings using the WAMES algorithm as proposed in (Vullings et al. 2009), which uses a dynamic mECG subtraction method to extract the fECG. Only files in which the fetal signal quality permitted reliable manual annotation of fetal R-peaks were selected, allowing for

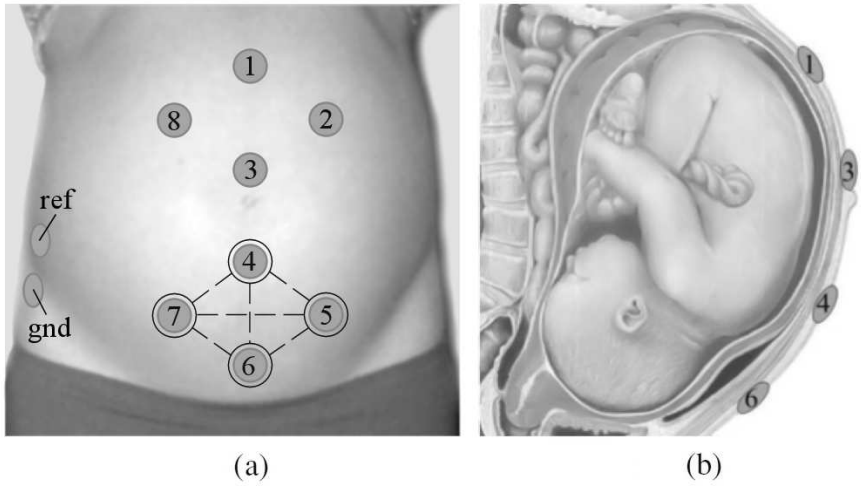

Figure 5. Electrode configuration: (a) front view and (b) side view, showing the locations of all electrodes, including reference (ref) and ground (gnd), as well as the bipolar leads (dashed lines) used for maternal R-peak detection.

comparison of fetal R-peak detection rates. The resulting fetal in-house database (fIHDB) comprises 6 recordings recorded at a gestational age of $41d0 \pm 5$, with a total length of 1.3 hours.

4.2. Detection performance

The detection performance of the algorithms is described as a combination of detection quality and detection accuracy. The detection quality is quantified by the detection error rate (D_e) of the algorithm to allow for a comparison with other algorithms from the literature. D_e is defined as:

$$D_e = \frac{FP + FN}{TP + FN}, \tag{25}$$

where TP is the number of correctly detected peaks (true positive), FN is the number of missed peaks (false negative), and FP is the number of falsely detected peaks (false positive). In line with previous studies, a peak is considered to be correctly detected if it is located within a ± 100 ms interval around the annotated peak position (Madeiro et al. 2007, Meyer et al. 2006). The detection accuracy is determined by the mean ($E[\Delta]$) and standard deviation (σ) of the offset between all correctly detected peaks and the reference annotations.

4.3. Computational complexity

The average number of multiplications per sample (MPS) is used as a measure of computational complexity of each of the algorithms. This measure is used because the number of computation cycles in a DSP is indicative of the energy consumption. Since on most low-power DSPs a multiplication is the most complex hardware accelerated

computation, all operations with a complexity higher than a multiplication (m), e.g. a division or square root, are executed using multiple multiplications and/or other instructions. Assuming the use of a 16-bit DSP, like the Ultra-Low-Power C5000$^{\text{TM}}$ series by TI, the higher complexity operations can be mapped to a fixed number of multiplications. Both the division and square root operations have a complexity in the order of $m \cdot O[n]$, where n is the precision of a value in number of bits. Therefore, assuming maximal precision for both numerator and denominator, a division and square root can be substituted by 9 and 17 multiplications, respectively (Robison 2005). All simple operations, e.g. addition, subtraction or bit-shift, are left out of consideration.

5. RESULTS

Fig. 6 shows an example of an ECG signal segment including the locations of maternal and fetal R-peaks, as well as the corresponding output of the preprocessing stage and thresholds used by the proposed R-peak detection algorithm.

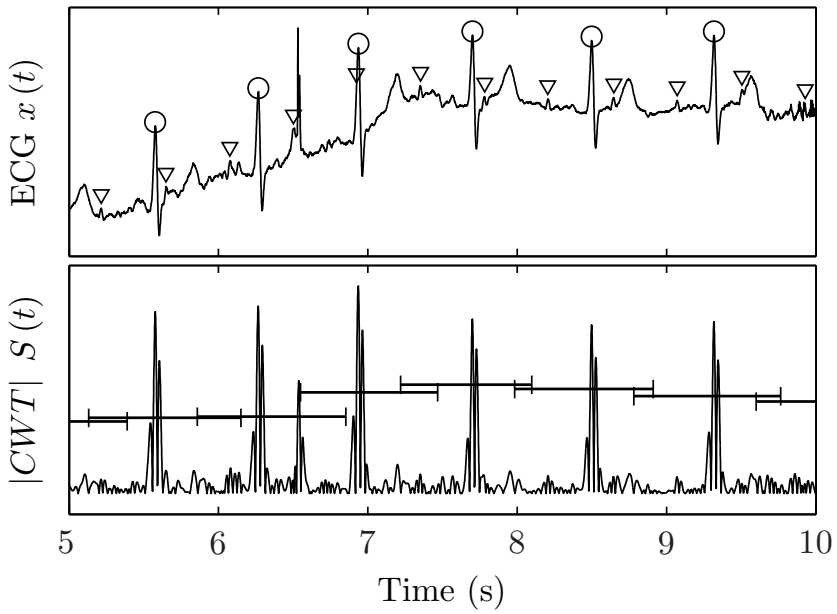

Figure 6. Example of an ECG segment (top), where $\odot$ and ∇ indicate the maternal and fetal R-peaks respectively, The horizontal bars in the preprocessing output (bottom) indicate the threshold level and length of each segment.

Table 2 shows a comparison of recent state-of-the-art R-peak detection algorithms on both detection performance and computational complexity for the MITDB. The computational complexity for each of the algorithms is estimated using available MATLAB code. As can be seen in Table 2, the D_e results of the Matlab implementations for both (Vullings et al. 2009) and (Pan & Tompkins 1985) closely resemble the published results. Despite our best efforts, however, the D_e of our implementation of (Li et al. 1995) on the MITDB does not reproduce the published result.

Table 2. Comparison of the presented algorithm with algorithms from the literature on the MITDB

	D_e (%)[b]	D_e (%)[c]	$E[\Delta] \pm \sigma$ (ms)[c]	MPS
(Li et al. 1995) [a]	0.17	0.80	-0.6 ± 13.9	140
This work	**0.23**	**0.23**	**0.2 ± 7.8**	**60**
(Vullings et al. 2009)	0.56	0.56	-2.2 ± 9.5	259
(Pan & Tompkins 1985) [a]	0.71	0.71	-5.5 ± 9.2	72

[a] D_e recomputed due to discrepancy in presented results.
[b] Calculated from values in paper.
[c] From best effort implementation based on paper.

Table 3. Comparison of D_e in % of the presented algorithm with best-effort implementations of (Vullings et al. 2009, Li et al. 1995, Pan & Tompkins 1985) on all bipolar leads in the IHDB

	Bipolar leads					
	$5-4$	$6-4$	$7-4$	$6-5$	$5-7$	$6-7$
(Li et al. 1995)	5.58	14.26	11.32	7.29	3.53	10.77
This work	**2.19**	**6.93**	**7.86**	**2.93**	**1.32**	**6.03**
(Vullings et al. 2009)	5.89	9.73	9.54	9.38	5.62	11.74
(Pan & Tompkins 1985)	5.47	15.67	12.73	7.76	3.89	13.23

Table 4. Comparison of the presented R-peak detection algorithm and best-effort implementations of (Vullings et al. 2009, Li et al. 1995, Pan & Tompkins 1985) on both the IHDB and fIHDB

		D_e (%)	$E[\Delta] \pm \sigma$ (ms)	MPS
IHDB	(Li et al. 1995)	3.53	-1.5 ± 6.8	300
	This work	**1.32**	**2.5 ± 3.3**	**135**
	(Vullings et al. 2009)	5.62	0.2 ± 7.0	595
	(Pan & Tompkins 1985)	3.89	-2.6 ± 5.0	150
fIHDB	(Li et al. 1995)	18.72	-0.6 ± 22.5	190
	This work	**9.42**	**2.2 ± 15.5**	**80**
	(Vullings et al. 2009)	19.23	-5.7 ± 20.3	380
	(Pan & Tompkins 1985)	10.79	-1.1 ± 16.4	95

Table 3 shows a comparison in detection quality between (Vullings et al. 2009, Li et al. 1995, Pan & Tompkins 1985) and the presented algorithm for all bipolar leads in the IHDB. The best bipolar lead for all of the algorithms (5-7) is used in Table 4, which shows a comparison in both detection performance and computational complexity between the various algorithms on both the IHDB and fIHDB.

6. DISCUSSION & CONCLUSION

A high-quality computation-efficient R-peak detection algorithm was developed based on the DT-CWT, combining high quality R-peak detection with a low computational complexity. Results show that the presented algorithm has an R-peak detection rate comparable to or better than other state-of-the-art algorithms in literature, at a reduced computational complexity. Additionally, the detection accuracy of the R-peak positions is higher than that of the other algorithms. For both the MITDB and IHDB, this difference is statistically significant. Compared to the R-peak detection algorithm in (Vullings et al. 2009), a decrease in D_e over 50% and an 75% reduction in computational complexity on both thoracic as well as maternal and fetal abdominal measurement data is obtained. The overall computational complexity of the algorithm is low because of the application of the DT-CWT, using a Mexican hat wavelet at a single scale and minimal postprocessing. Despite this, a high detection rate is achieved due to the use of dynamic segmentation, SNR dependent thresholding, and an optimal wavelet shape which was found after evaluating various wavelets.

Only the algorithm by (Li et al. 1995) achieves, according to the literature, a slightly higher detection rate on the MITDB than the presented algorithm. Despite our best efforts, however, we were unable to reproduce these results on the MITDB, which might impact the results of the determined D_e for Li's algorithm on the abdominal datasets. Also, because of the use of the discrete wavelet transform (DWT) with a quadratic-spline wavelet at multiple scales, as well as significant postprocessing, the complexity of (Li et al. 1995) is higher than that of the presented algorithm. Furthermore, DT-CWT R-peak detection methods are claimed to be more robust to noise than the DWT as used by Li, making the proposed algorithm more suitable for use in an ambulatory setting (Romero et al. 2009). Noteworthy is also the relatively good performance of the Pan-Tompkins algorithm on the fIHDB, the most noisy of the datasets. This might be due to the method of threshold calculation, which, similar to the presented algorithm, is recalculated after every detected peak and takes into account both the amplitude of the detected QRS-complexes as well as those of the noise peaks.

When used as part of the WAMES algorithm (Vullings et al. 2009), the proposed R-peak detection algorithm allows for real-time detection of fetal R-peaks, outperforming other abdominal ECG based techniques, like ICA. Unlike Doppler ultrasound based techniques which smoothen the fHR signal, the proposed method can provide the fHR on a beat-to-beat basis. This enables an accurate spectral analysis of the fHR since high-frequency components are preserved. Additionally, unlike Doppler ultrasound, no energy is introduced into the body, reducing power consumption.

In conclusion, the presented algorithm shows high-quality detection results for both maternal and fetal R-peaks at a low computational complexity, allowing for continuous ambulatory monitoring. The signals in the used datasets were, however, recorded while the patient was stationary. In an ambulatory setting, artifacts will become more predominant and despite the improvement in detection performance over

other R-peak detection algorithm, the proposed algorithm is still susceptible to motion artifacts. Additional work is necessary before reliable ECG detection is feasible in a truly ambulatory setting.

Our future work will therefore include validation of the algorithm on a new dataset, recorded in an ambulatory setting on subjects with a wide range of gestational age. The R-peak detection algorithm will then be optimized for high detection performance in noisy recordings, due to the changes in the signal characteristics and additional motion artifacts, while retaining a low complexity. Additionally, a reduction in complexity of the mECG estimation and subtraction is needed prior to implementation on a low-power mobile platform.

Acknowledgments

This work was supported by the Dutch Technology Foundation STW

References

Abboud S & Sadeh D 1989 *Computers in Biology and Medicine* **19**(6), 409 – 415.

Addison P S 2002 *The Illustrated Wavelet Transform Handbook* IOP Publishing.

Amer-Wahlin I, Hellsten C, Norn H, Hagberg H, Herbst A, Kjellmer I, Lilja H, Lindoff C, Mansson M, Martensson L, Olofsson P, Sundstrm A K & Marsl K 2001 *The Lancet* **358**(9281), 534 – 538.

Bergveld P & Meijer W J H 1981 *IEEE Trans. Biomed. Eng.* **BME-28**(4), 348 –354.

Dawes G, Moulden M & Redman C 1990 *International Journal of Bio-Medical Computing* **25**(4), 287 – 294. ¡ce:title¿Workshop on Personal Computer Based Analysis of Fetal Heart Rate¡/ce:title¿.

Graatsma E M, Jacod B C, Van Egmond L A J, Mulder E J H & Visser G H A 2009 *BJOG* **116**, 334 – 338.

Gritzali F 1988 *Sig. Proc.* **15**(2), 183 – 192.

Gritzali F, Frangakis G & Papakonstantinou G 1989 *Computers and Biomedical Research* **22**(1), 83 – 91.

Haritopoulos M, Capdessus C & Nandi A 2010 *in* 'Engineering in Medicine and Biology Society (EMBC), 2010 Annual International Conference of the IEEE' pp. 1910 –1913.

Hon E H, Paul R H & Hon R W 1972 *BJOG* **40**, 362–365.

Kieler H, Cnattingius S, Haglund B, Palmgren J & Axelsson O 2001 *Epidemiol.* **12**(6), 618 – 623.

Kohler B U, Hennig C & Orglmeister R 2002 *IEEE Eng. Med. Biol. Mag.* **21**(1), 42 – 57.

Li C, Zheng C & Tai C 1995 *IEEE Trans. Biomed. Eng.* **42**(1), 21 – 28.

Madeiro J P, Cortez P C, Oliveira F I & Siqueira R S 2007 *Med. Eng. & Phys.* **29**(1), 26 – 37.

Martinez J, Almeida R, Olmos S, Rocha A & Laguna P 2004 *IEEE Trans. Biomed. Eng.* **51**(4), 570 – 581.

Martinez J, Olmos S & Laguna P 2000 *in* 'Computers in Cardiology' pp. 81 –84.

Meyer C, Gavela J & Harris M 2006 *IEEE Trans. Inf. Technol. Biomed.* **10**(3), 468 – 475.

Moody G B 1997 'MIT/BIH arrhythmia database'.
URL: *http://physionet.org/physiobank/database/mitdb/*

Pan J & Tompkins W J 1985 *IEEE Trans. Biomed. Eng.* **32**(3), 230 – 236.

Peters M, Crowe J, Piri J F, Quartero H, Hayes-Gill B, James D, Stinstra J & Shakespeare S 2001 *Journal of Perinatal Medicine* **29**(5), 408–416.

Rabotti C, Mischi M, van Laar J O E H, Oei G S & Bergmans J W M 2009 *Phys. Meas.* **30**(8), 745 – 761.

Robergs R A & Landwehr R 2002 *Official Journal of The American Society of Exercise Physiologists* **5**(2), 1–10.

Robison A 2005 *in* 'ARITH-17 2005' pp. 131 – 139.

Romero I, Grundlehner B, Penders J, Huisken J & Yassin Y 2009 *in* 'IEEE BioCAS 2009' pp. 249 –252.

Romero Legarreta I, Addison P S, Reed M J, Grubb N, Glegg G R, Robertson C E & Watson J N 2005 *Int. Journal of Wavelets* **3**, 19 – 42.

Sahin I, Yilmazer N & Simaan M 2010 *IEEE Trans. Biomed. Eng.* **57**(4), 875 – 883.

Strobach P, Abraham-Fuchs K & Harer W 1994 *IEEE Trans. Biomed. Eng.* **41**(4), 343 –350.

Taylor M J, Smith M J, Thomas M, Green A R, Cheng F, Oseku-Afful S, Wee L Y, Fisk N M & Gardiner H M 2003 *BJOG* **110**(7), 668–678.

Taylor M J, Thomas M J, Smith M J, Oseku-Afful S, Fisk N M, Green A R, Paterson-Brown S & Gardiner H M 2005 *BJOG* **112**(8), 1016–1021.

Ungureanu M, Bergmans J W, Oei S G & Strungaru R 2007 *Biomedical Engineering* **52**.

Vullings R, Peters C H L, Sluijter R J, Mischi M, Oei S G & Bergmans J W M 2009 *Phys. Meas.* **30**(3), 291 – 307.

Widrow B, Glover, J.R. J, McCool J, Kaunitz J, Williams C, Hearn R, Zeidler J, Eugene Dong J & Goodlin R 1975 *IEEE proceedings* **63**(12), 1692 – 1716.

Yoon U J, Hwang I S, Noh Y S, Chung I C & Yoon H R 2010 *in* 'ICWAPR 2010' pp. 300 –303.